(2)

SECURITY CLASSIFICATION OF THIS PAGE

REPORT DOCUMENTATION PAGE

AD-A220 142

1a REPORT SECURITY CLASSIFICATION: Unclassified	1b RESTRICTIVE MARKINGS: None
	3 DISTRIBUTION/AVAILABILITY OF REPORT: Approved for Public Release, Distribution Unlimited
4 PERFORMING ORGANIZATION REPORT NUMBER(S): Technical Report #6	5 MONITORING ORGANIZATION REPORT NUMBER(S)
6a NAME OF PERFORMING ORGANIZATION / 6b OFFICE SYMBOL (If applicable)	7a NAME OF MONITORING ORGANIZATION: ONR
6c ADDRESS (City, State, and ZIP Code)	7b ADDRESS (City, State, and ZIP Code): 800 North Quincy Avenue Arlington, VA 22217
8a NAME OF FUNDING/SPONSORING ORGANIZATION: ONR / 8b OFFICE SYMBOL (If applicable)	9 PROCUREMENT INSTRUMENT IDENTIFICATION NUMBER
8c ADDRESS (City, State, and ZIP Code): 800 North Quincy Avenue Arlington, VA 22217	10 SOURCE OF FUNDING NUMBERS: PROGRAM ELEMENT NO. / PROJECT NO. / TASK NO. / WORK UNIT ACCESSION NO.

11 TITLE (Include Security Classification)
Dynamics of Microphase Separation During RIM Copolymerization; Some Synchrotron SAXS Experiments

12 PERSONAL AUTHOR(S)
A.J. Ryan, W.R. Willkomm, T.B. Bergstrom, C.W. Macosko, J.T. Koberstein and T.P. Russell

13a TYPE OF REPORT	13b TIME COVERED	14 DATE OF REPORT (Year, Month, Day)	15 PAGE COUNT
Technical	FROM _____ TO _____	1990.3.27	3

16 SUPPLEMENTARY NOTATION
Presented at Macromolecules '89 Second Euro-American Conference on Functional Polymers and Biopolymers, Aug. 5-8, Oxford, U.K.

17 COSATI CODES			18 SUBJECT TERMS (Continue on reverse if necessary and identify by block number)
FIELD	GROUP	SUB-GROUP	

19 ABSTRACT (Continue on reverse if necessary and identify by block number)

Using the high x-ray flux afforded by a synchrotron radiation source, the formation of the polyurethane morphology during fast polymerization by reaction injection molding (RIM) was observed as a function of mold temperature through small angle x-ray scattering measurements. To our knowledge, this represents the first time that the development and growth of microphase separation during the polyurethane RIM process has been reported.

20 DISTRIBUTION/AVAILABILITY OF ABSTRACT: ☒ UNCLASSIFIED/UNLIMITED ☐ SAME AS RPT ☐ DTIC USERS	21 ABSTRACT SECURITY CLASSIFICATION: None
22a NAME OF RESPONSIBLE INDIVIDUAL: J.T. Koberstein	22b TELEPHONE (Include Area Code): (203) 486-4716 / 22c OFFICE SYMBOL

DD FORM 1473, 84 MAR — 83 APR edition may be used until exhausted. All other editions are obsolete

SECURITY CLASSIFICATION OF THIS PAGE

OFFICE OF NAVAL RESEARCH

Contract N00014-86-K-0497

R&T Code 4132013

Technical Report No. 6

Dynamics of Microphase Separation During RIM Copolymerization; Some Synchrotron SAXS Experiments

by

A. J. Ryan, W. R. Willkomm, T. B. Bergstrom, and C. W. Macosko,
J. T. Koberstein, and T. P. Russell

Presented at Macromolecules '89, Second Euro-American Conference on Functional Polymers and Biopolymers, 5-8 August 1989, Oxford U.K.

University of Connecticut
Institute of Materials Science
and Department of Chemical Engineering
Storrs, CT 06269-3136

March 27, 1990

Macromolecules '89
Second Euro-American Conference on Functional Polymers and Biopolymers
5-8 Aug, Oxford, UK, 1989

DYNAMICS OF MICROPHASE SEPARATION DURING RIM COPOLYMERIZATION: SOME SYNCHROTRON SAXS EXPERIMENTS

A.J. Ryan*, W.R. Willkomm, T.B. Bergstrom and C.W. Macosko, University of Minnesota, Minneapolis, MN 55455, USA.
J.T. Koberstein, University of Connecticut, USA and
T.P. Russell, IBM, San José, USA

Introduction

Reaction injection molding (RIM) is a well established process for the production of polymeric articles by simultaneous shaping and polymerization. The major polymers produced by this process (but not all) are segmented block copolymers . In contrast to other polymer processes the build up of mechanical properties occurs by phase separation and this competes with the copolymerization.

The ultimate properties of RIM materials are drastically affected by their molecular weight and morphology. Depending on the route the polymerizing mixture takes through phase space, two macrophase separation mechanisms may be observed, namely, nucleation and growth (N & G) or spinodal decomposition (SD). In both the cases phase separation proceeds until one phase vitrifies and/or crystallizes; the SD mechanism can lead to the formation of nonequilibrium morphologies which comprise two interpenetrating networks whereas the N & G mechanism tends to form continuous-phase/discontinuous-phase morphologies[1]. Very early phase separation can limit molecular weight buildup by separating reactive groups. If a segmented block copolymer is formed prior to macrophase separation of a polymerizing mixture, microphase separation may occur.

The kinetics of phase separation may be followed by SAXS if the copolymerizing materials possess sufficient contrast (the square of the electron density difference). Spinodal decomposition has a definite scattering signature: Cahn's linearized theory predicts that the composition gradients, and thus scattered intensity, have a maximum for a given wavenumber and that in the early stages of the decomposition there is an exponential increase in the scattered intensity with time. The nucleation and growth process is not very well defined in terms of a kinetic scattering theory, however, the scattered intensity has been observed to depend on time squared for well characterized N&G systems.

The high flux of synchrotron radiation is required in order to permit real time study of the kinetics of phase separation. The spatial resolution and signal to noise ratio of Beam Line 1-4 at the Stanford Synchrotron Research Laboratory (SSRL) permits analysis of the full SAXS profile ~10 times every second and thus meaningful kinetic data may be obtained. For example, one of the most interesting phase separating copolymerizations is complete in ~2 seconds and proceeds from a liquid with a viscosity of ~1 Pa s to a solid with a modulus of ~1 GPa in this time frame; other systems can take up to fifteen minutes to become completely phase separated. In comparison, conventional Kratky Camera technology requires that data over a period of ~10 hours be averaged to obtain a scattering profile with good signal to noise ratio for RIM materials, thus the kinetics of phase separation may not be investigated by this technique

Experimental

A MicroRIM machine was used to meter and mix small (~10 g) stoichiometric quantities of reactive monomers and deliver them to the analytical instrument. This equipment has been designed and developed at the University of Minnesota over a period of years and has proved to be safe and reliable[2]. A specially designed cell with Kapton polyimide windows was constructed. It has a very small volume, to permit fast filling, and can be placed, reproducibly in a heating block attached to a optical bench. The white light emanating from the synchrotron storage ring is focussed by means of a float glass mirror and a bent, asymmetrically cut, Si(111) crystal. The Si monochromator was adjusted to deliver 1.429 Å X-rays. The incident-beam profile is defined with a number of antiscatter slits to give a cross section of approximately 1mm^2 at the sample position. Scintillation detectors placed before and after the the sample cell record the incident and transmitted intensities by diffraction from 10 mm thick Kapton windows inclined at 45 ° with respect to the incident radiation, thus changes in the specimens attenuation factor are monitored continuously. The detector is a 1024 pixel EG&G Reticon photodiode array cooled to ~-80 °C and placed several centimeters behind the focal spot of the X-rays. The detector assembly is interfaced with a DEC 11/34 computer via CAMAC electronics[3]. The photodiode array is scanned every 25.6 ms and at least 30 signals must be averaged before being written to disc.

Results and discussion

The chemical system selected for these initial experiments was the well characterized polyurethane based on methylene-bis-4,4'-phenyl isocyanate (MDI), butan-1,4-diol(BDO) and a 2000 polyether diol. Complete analysis of the data is still ongoing though a qualitative description of the process may be obtained from inspection of the raw pixel number versus relative intensity curves. Experiments were conducted at four different cell temperatures for a 48% hard segment formulation containing .02% dibutyl tin dilaurate. The results are shown schematically in Figure 1.

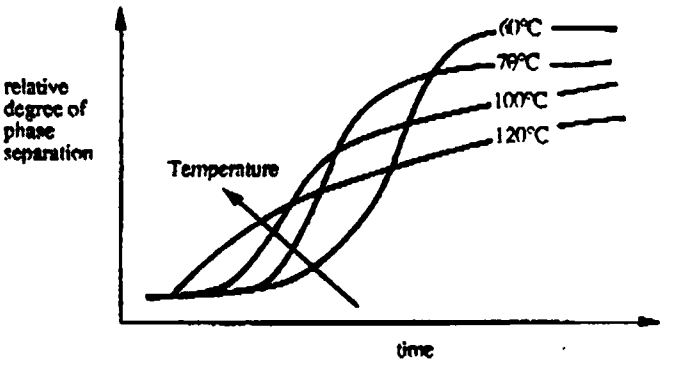

Figure1. A schematic representation of the SAXS results for MDI/BDO/diol system

The overall trend was that higher temperatures caused phase separation to be faster whereas at lower temperatures the degree of phase separation achieved was greater. Materials formed with a cell temperature >100 °C appeared to crystallize from a homogenous melt whereas the materials formed at cell temperatures of <100 °C appeared to phase separate before crystallization. Qualitatively the data are in good agreement with the main trends of Yang's[4] work on RIM dynamics, however, SAXS studies of the 4,4' MDI/BDO/diol systems are impaired by the onset of hard segment crystallization swamping phase separation and unambiguous identification of the phase separation process was not possible.

We are investigating three approaches to the problem: (i) reproducing some of Yang's experiments on the synchrotron, (ii) generating new rheological and FTIR data for 2,4 MDI/BDO/diol materials which will be amenable to unambiguous SAXS experiments and (iii) developing new model polyurea chemistries which are amenable to real-time SAXS analysis and parallel quenching experiments on preformed block copolymers. This work will also be reported.

References

1. O. Olabisi, L.M. Robeson and M.T. Shaw, "Polymer-Polymer Miscibility" Academic Press, New York, 1979.
2. K. Mikkleson and C.W. Macosko, J. Elast. Plast., 1989, 21, 29.
3. J.T. Koberstein and T.P. Russell, Macromolecules, 1986, 19, 714.
4. W.P. Yang, PhD Thesis, University of Minnesota, 1988

Figure 2. Schematic of sample cell

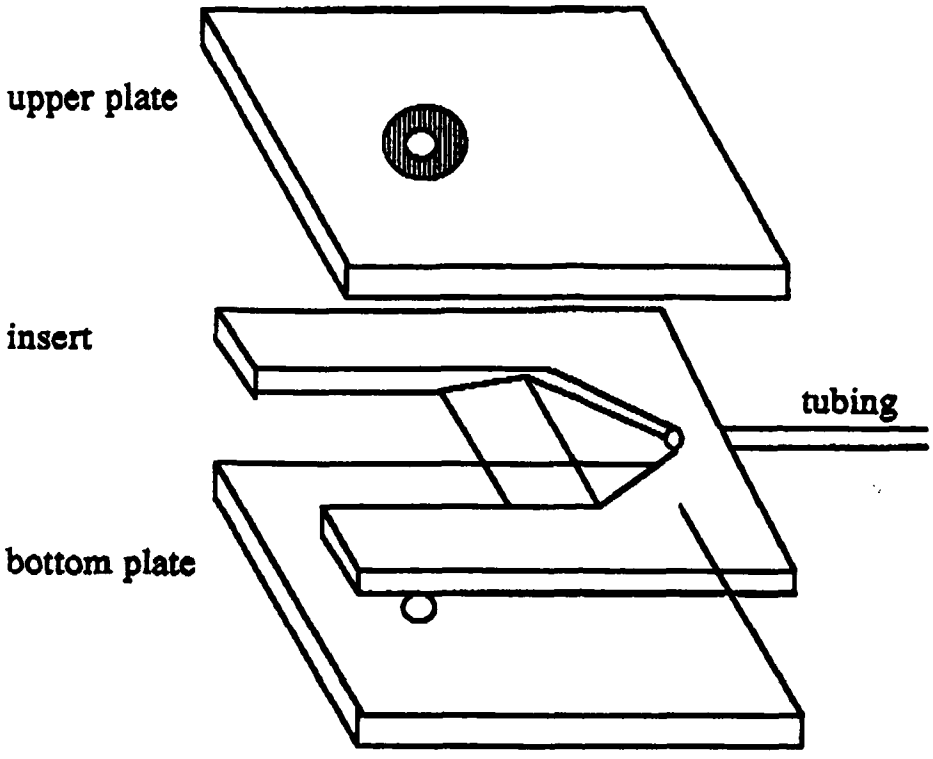

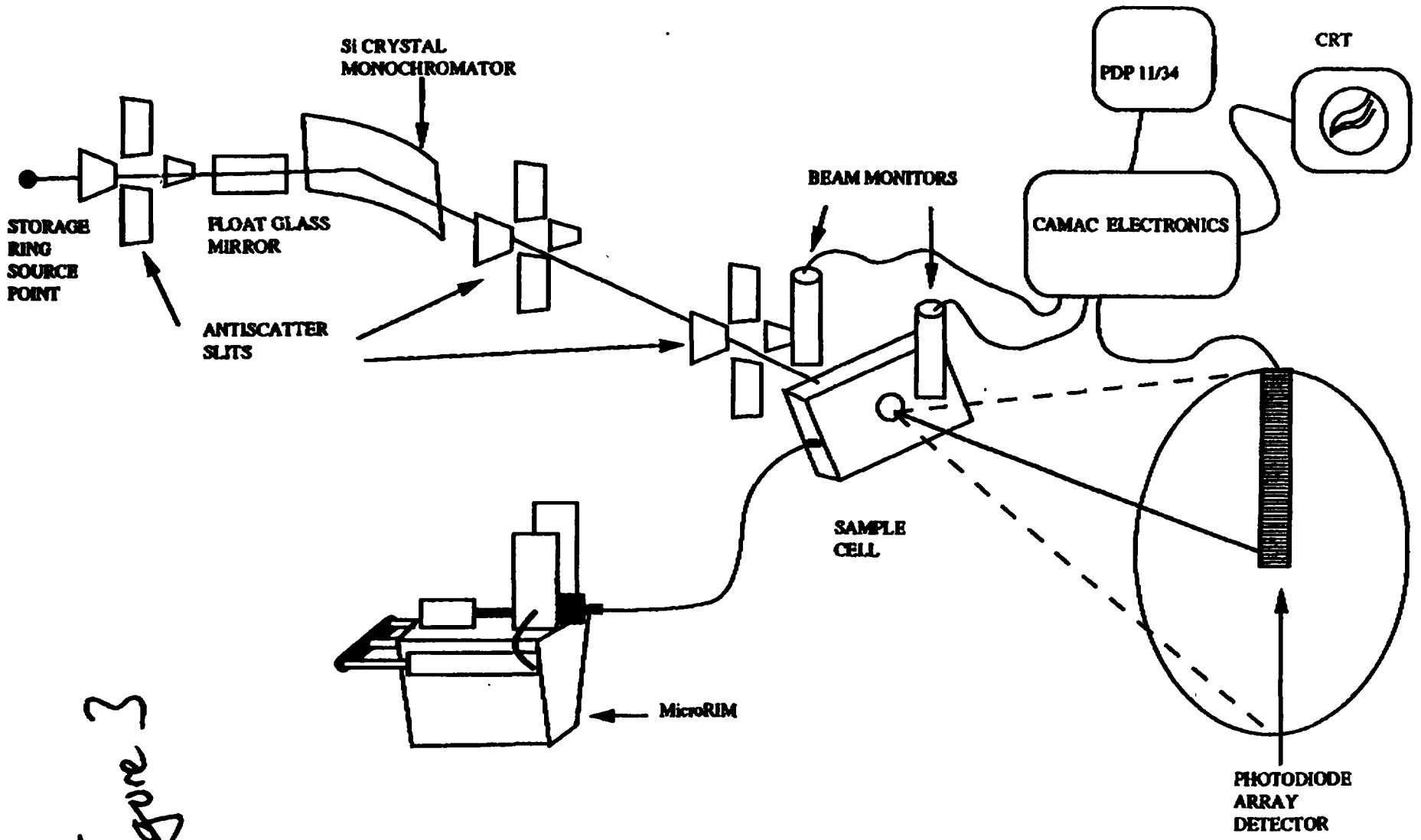
Si CRYSTAL
MONOCHROMATOR
PDP 11/34
CRT
BEAM MONITORS
CAMAC ELECTRONICS
STORAGE
RING
SOURCE
POINT
FLOAT GLASS
MIRROR
ANTISCATTER
SLITS
SAMPLE
CELL
MicroRIM
PHOTODIODE
ARRAY
DETECTOR

Figure 3